Inhibiting *Mycobacterium tuberculosis* ClpP1P2 by addressing the equatorial handle domain of ClpP1 subunit

Yang Yang[1#], Yibo Zhu[1#], Tao Yang[1#], Tao Li[1], Yuan Ju[1], Yingjie Song[1], Jun He[1], Huanxiang Liu[2], Rui Bao[1*] and Youfu Luo[1*]

[1] Center of Infectious Diseases, State Key Laboratory of Biotherapy, West China Hospital, Sichuan University, Chengdu, 610041, China

[2] School of Pharmacy, Lanzhou University, Lanzhou, 730000, China

*Address correspondence to R.B. and Y.F.L.

E-mail: baorui@scu.edu.cn; luo_youfu@scu.edu.cn

# These authors contributed equally to this work.

Abstract

Unlike other bacterial ClpP systems, mycobacterial ClpP1P2 complex is essential for mycobacterial survival. The functional details of *Mycobacterium tuberculosis* (*Mtb*) ClpP1P2 remains largely elusive and selectively targeting ClpP of different species is a big challenge. In this work, cediranib was demonstrated to significantly decrease the activity of *Mtb*ClpP1P2. By solving the crystal structure of cediranib-bound *Mtb*ClpP1P2, we found that cediranib dysregulates *Mtb*ClpP1P2 by interfering with handle domain of the equatorial region of *Mtb*ClpP1, indicating that the inter-ring dynamics are crucial for its function. This finding provides direct evidence for the notion that a conformational switch in the equatorial handle domain is essential for ClpP activity. We also present biochemical data to interpret the distinct interaction pattern and inhibitory properties of cediranib toward *Mtb*ClpP1P2. These results suggest that the variable handle domain region is responsible for the species-selectivity of cediranib, which suggests the equatorial handle domain as a potential region for screening pathogen-specific ClpP inhibitors.

Introduction

Caseinolytic protease ClpP, a widely conserved self-compartmentalizing serine protease in bacteria, plays essential roles in protein metabolism and regulates diverse physiological functions including cell motility, genetic competence, cell differentiation, sporulation, and virulence, and is thus an attractive target for antibiotic development[1-8]. Notably, ClpP is an novel drug target for which both inhibition and activation result in an attenuated or lethal phenotype in many pathogens; thus agonists and antagonists

aimed at the ClpP system represent promising drug candidates for further evaluation[9, 10]. The ClpP enzyme of *Mycobacterium tuberculosis (MTB), Mtb*ClpP1P2, exerts its proteolytic function by a heterotetramer of two protein subunits, ClpP1 and ClpP2[11, 12]. Moreover, encoding genes of subunits ClpP1 and ClpP2, have been shown to be essential genes for *MTB* survival and the deletion of either gene causes bacterial death[13]. A panel of *Mtb*ClpP1P2 inhibitors have been reported and they can be classified into two categories depending on their action modes. The first kind of small molecules act on the catalytically active center, covalently modifying the serine residues of the active sites of two subunits of *Mtb*ClpP1P2, including bortezomib, boron-containing analogues and beta lactones[14-17]. The second kind of inhibitors act on the chaperone protein (ClpX/ClpC1) binding site that competitively binds to the surface of the ClpP2 subunit. Representative molecules of this category are ADEP and its analogs[12]. Since the chaperones binding L/IGF region of ClpP2 subunit is highly conserved, as with the inhibitor of the *Mtb*ClpP1P2 catalytic center[18], the ADEP compounds are nonselective as well. As we know, the off-target effects may bring severe side effects during drug development. Thus it is desirable to find novel binding pocket or selective inhibitors targeting *Mtb*ClpP1P2 to avoid the potential adverse effects of nonselective ones. In this work, we demonstrate that cediranib, an orally available vascular endothelial growth factor receptor 2 (VEGFR-2) inhibitor, is able to inhibit *Mtb*ClpP1P2 peptidase activity. We solved the crystal structure of *Mtb*ClpP1P2 in complex with an agonist peptide and cediranib, and present details of the inhibitory mechanism. Unlike other ClpP inhibitors, cediranib dysregulates *Mtb*ClpP1P2 by

63 interfering with the equatorial region of *Mtb*ClpP1, supporting the idea that the inter-
64 ring dynamics are crucial for ClpP function. We also present biochemical data
65 suggesting that this mechanism is distinct from those of previously reported ClpP
66 inhibitors. These results reveal a novel druggable pocket in *Mtb*ClpP1P2, with potential
67 implications for further research on ClpP catalytic mechanism and drug development.

68 # Results

69 ## Identification of cediranib as a novel inhibitor of *Mtb*ClpP1P2

70 We screened about 2600 bioactive compounds (MedChemExpress, HY-L001)
71 based on a peptidase activity assay. Eight compounds (hit rate 0.31%) that generated
72 ≥80% inhibition of *Mtb*ClpP1P2 were selected for IC_{50} value evaluation (Fig 1A).
73 Among these hits, cediranib and brivanib, which possesses an indolyl group, showed
74 promising inhibitory effects toward *Mtb*ClpP1P2 peptidase activity; cediranib had a
75 lower IC_{50} value (3.4 μM) than brivanib (12.5 μM) (Fig 1A and 1B). In addition,
76 cediranib (100μM) led to a peak shift of 10°C in the thermal stability of *Mtb*ClpP1P2
77 in differential scanning calorimetry (DSC) assay, which confirms their direct interaction
78 in solution (S1 Fig).

79 To dissect whether cediranib is a species-selective inhibitor, we profiled its
80 peptidase inhibitory effects against a panel of ClpPs from *Escherichia coli* (*Ec*ClpP),
81 *Pseudomonas aeruginosa* (*Pa*ClpP1), and *Staphylococcus aureus* (*Sa*ClpP) (Table 1
82 and S2 Fig). The results show that cediranib has no obvious inhibitory effect on those
83 ClpP variants. In contrast, cediranib demonstrated non-competitive inhibition of
84 *Mtb*ClpP1P2 (Fig1C), indicating that it may not form covalent bonds with the protease.

To validate the antibacterial activity of cediranib, we carried out growth inhibition assays on several pathogenic bacteria. As Table 1 and Table 2 show, cediranib had no inhibitory activity toward *S. aureus*, *P. aeruginosa*, *Escherichia coli* and *Enterococcus faecalis* (minimum inhibitory concentration [MIC] >128 μg/mL), while it was toxic to *E. faecium*, *Staphylococcus epidermidis*, *Klebsiella pneumoniae* and *Mycobacterium smegmatis* MC^2155 (MIC 64 μg/mL). Cediranib inhibited the growth of *Mtb* H37Rv with an MIC value of 16 μg/mL. Therefore, cediranib exhibits species-selectivity in suppressing pathogen growth. Next, we performed peptidase assay on human ClpP (*h*ClpP) to estimate the toxicity of cediranib to human mitochondria. As shown in Table 1 and S2 Fig, cediranib displayed weak inhibition of *h*ClpP activity compared to *Mtb*ClpP1P2, with a selectivity index >10.

To gain insights into the inhibitory mechanism of cediranib, we purified and crystallized *Mtb*ClpP1P2 in complex with cediranib and benzoyl-Leu-Leu (Bz-LL). The crystals belonged to space group C121 and diffracted to 2.7 Å resolution. The structure was determined by molecular replacement using the previously solved *Mtb*ClpP1P2 structure (PDB code 5DZK) as a search model, and the final model was refined to an Rfactor of 20.02% (Rfree =24.33%) (Table 3)[19]. The asymmetric unit has one hetero-tetradecameric complex structure composed of heptameric ClpP1 and ClpP2 rings (Fig 2A). The organization and overall structure remain identical to those in benzyloxycarbonyl-Ile-Leu (Z-IL)-bound and Bz-LL-bound *Mtb*ClpP1P2 structures[12, 19], presenting an open-pore conformation with 30 and 25 Å diameters in the ClpP1 and P2 rings, respectively (Fig 2B).

*Mtb*ClpP1 and *Mtb*ClpP2 share high sequence identity (48%) and have a common core structure, which adopts an α/β-fold consisting of two central twisted β-sheets flanked by seven α-helices and an extended handle domain (Fig 2C). The N-terminal regions of *Mtb*ClpP2 are in an extended β-hairpin conformation, and are further stabilized by the *Mtb*ClpP2 ring from the crystallographic symmetry unit. The typical catalytic triad (Ser-His-Asp) locates in the cleft between the core domain and the handle domain; all 14 active sites distribute on the inner surface of the assembled *Mtb*ClpP1P2 complex and eventually form the hydrolytic chamber. Bz-LL peptides occupied all cleavage centers in the *Mtb*ClpP1ClpP2 tetradecamer, whereas seven cediranib molecules bound within the cleft between *Mtb*ClpP1 monomers.

Self-association is a common and well-conserved property of Clp protease. The inter-ring interactions are mediated by the handle domain, a strand-turn-helix motif that forms the equatorial regions of the ClpP barrel[20-24]. Compared with the Bz-LL-bound *Mtb*Clp1Clp2 structure[19], the additional binding of cediranib slightly reduced the interface area between *Mtb*ClpP1 monomers (from 1356 Å2 to 1116 Å2), but does not change the assembly state of the whole complex, suggesting that the inhibitory mechanism of cediranib is different from that of compounds that disrupt the oligomerization of the ClpP complex[25].

Cediranib-bound *Mtb*ClpP1P2 structure reveals a novel inhibitor binding-site

As previously reported[12, 19], the binding sites of Bz-LL and Z-IL are aligned parallel to β-strands 6 and 8 in each subunit and the agonist peptides form several hydrogen bonds with protein main-chain atoms. However, because *Mtb*ClpP2 has a

longer loop after the βG strand (residues 127–129) and thus generates a shallower S1 pocket, Bz-LL is bound in opposite orientations in *Mtb*ClpP1 and *Mtb*ClpP2 (Fig 3A), supporting the notion that *Mtb*ClpP1 and *Mtb*ClpP2 have different substrate specificities[26]. In *Mtb*ClpP1, around the Bz-LL binding site, the averaged 2Fo−Fc electron-density map allowed us to unambiguously build the cediranib molecules between α5 and α3 (Fig 3B and 3C). Cediranib binds this site predominantly via hydrophobic interactions, while its indolyl group forms a cation–π interaction with Arg119 (Fig 2D). Additionally, the quinazoline ring of cediranib interacts with the aromatic rings from Trp174 and the benzoyl group of Bz-LL, resembling a π–π stacking interaction. In contrast to *Mtb*ClpP1, the corresponding sites in *Mtb*ClpP2 generate a more compact pore, where α5 moves closer to α3 and the large side chains of Met160 and Phe83 restrict accessibility to this pocket, making cediranib unable to bind to *Mtb*ClpP2 (Fig 3D).

Unlike the peptidyl inhibitors that occupy the S1–S3 subsites of ClpP[27], cediranib does not directly interact with the active site, but interferes with the dynamic handle region, which was proposed to be responsible for product release[21, 28](Fig 3C and 3E). Though a small channel in the variable handle region of *Mtb*ClpP1 was observed in ADEP-*Mtb*ClpP1P2 complex in previous study[12], we firstly demonstrated this small channel could be occupied by a small molecule, herein cediranib, and be employed to realize *Mtb*ClpP selectivity. As Fig 3F illustrates, the cediranib-binding pocket is formed by α5 (residues Gln142–Glu149), α3 (residues Ile71–Ala76) and three short β-sheets (βD, βF, βH) from the neighboring ClpP1 subunit.

It is worth noting that α5 is the major part of the handle domain.

Molecular dynamics simulation studies revealed cediranib interferes the conformational changes of *Mtb*ClpP1

Previous molecular dynamics simulation studies on SaClpP revealed that α5 adopts a kinked conformation by breaking the helix at residue Lys145 (corresponding to Val145 in *Mtb*ClpP1)[24]. During the reaction cycle, the handle domain undergoes an unfolding/refolding process, allowing the whole cylindrical ClpP barrel to adopt extended, compact and compressed states[23, 24, 29-31]. In order to analysis the effect of cediranib on the dynamic transition of handle domain, we performed a 500-ns MD simulation on *Mtb*ClpP1 dimer (chain B and M) with/without cediranib (S3 Fig). The r.m.s. deviation (RMSD) values of Cα from the head domain and handle domain were monitored, the results indicated that handle domain underwent dramatic conformational changes during the simulation, whereas both the head domain and handle domian of B chain was more stable than that of M chain(S3A Fig and S3C Fig). Next, the secondary structure transformation of handle domain were calculated along the trajectory of simulation by DSSP[24] (S3B Fig and S3D Fig). The profile revealed that the N-terminal part of helix E (residues 133–158) underwent a helical unfolding/refolding process. In the absence of cediranib, the N-terminal part (residues 133–137) in chain B primarily adopted turn structure in 0-350 ns. Then, residues 133–154 adopted coil , turn and 3-10Helix structures. In chain M, residues 143–147 mainly adopted turn structure. With binding of cediranib, the N-terminal part(residues 133–137) of chain B adoped coil and turn strcture in the initial stage (0–300 ns). Subsequently(300-500ns), these

residues gradually readopted some 3-10Helix and α-helix. By contrast to chain B, chain M was much more unstable, particularly at 250ns, most α-helix structure adopted turn and coil (S3B Fig and S3D Fig). To identify the most significant motions of handle domain of *Mtb*ClpP1 dimer induced by cediranib, we performed PCA using the MD trajectory[24]. As shown in S3E Fig and S3F Fig, during the conformational transition, four intermediate conformations (see the 50-ns, 100-ns,300-ns, and 500-ns snapshots in Fig 3E and 3F) was observed. Based on the results of MD simulation and PCA, we constructed a rough energy landscape for the conformational transition of *Mtb*ClpP1 dimer projected onto the first two principal components, PC1 and PC2. Obviously, the binding of cediranib to *Mtb*ClpP1 interferes the conformational changes, likely preventing the protease from accomplishing the enzymatic process.

Mutagenesis and functional analysis of the cediranib-binding site

As we known, the ClpPs from different species share high sequence similarity (55.0–90.9%) and conserved overall structure (Fig 4A). Consistently, the general and critical gating mechanism of ClpP requires the handle domain to preserve its structural integrity[29]. In the dynamic region of the handle domain (Ser132–Val145 in *Mtb*ClpP1), several sites involved in structural stabilization have been identified to be important for ClpP function: Gln132/Glu135 in *Sa*ClpP (corresponding to Ser132/Asp135 in *Mtb*ClpP1, interacting with Arg171)[23]; Ile149/Ile151 in *Ec*ClpP (corresponding to Ile136/Ile138 in *Mtb*ClpP1)[21]; and Ala153 in *Streptococcus pneumoniae* ClpP (corresponding to Ala140 in *Mtb*ClpP1) (Fig 3F)[22]. Thus, the cediranib-bound *Mtb*ClpP1P2 structure provides additional evidence to highlight the

critical role of the handle region.

To investigate the residues in the cediranib-binding pocket, we introduced different mutations in relevant sites based on sequence alignment (Fig 4B and Table 4). Consistent with the importance of the equatorial pore and handle domain, most site-directed mutations in the selected sites decreased or abolished *Mtb*ClpP1P2 activity. Considering Ile71, Met75, Ile146 and Trp174, even when residues with similar side chains were substituted in those sites, the enzyme activity was not retained, suggesting there are constraints on both residue size and chemical properties to maintain the local structural integrity and flexibility (Table 4 and Fig 4C).

An electrostatic interaction between two *Mtb*ClpP1 subunits (Arg119–Gln142) (Fig 3F) seems to be an important factor mediating the side pore gating, because any substitution that changed the charge properties of either site resulted in reduced or abolished activity. In contrast, sites Met95 and Glu149 of *Mtb*ClpP1 exhibit various levels of tolerance to mutation. In particular, Met95Gln and Glu149Leu variants retain activity and have altered sensitivity of *Mtb*ClpP1P2 to cediranib, providing a structural basis for the specific recognition between cediranib and *Mtb*ClpP1 (Table 4).

Discussion

ClpP represents a unique type of serine protease complex responsible for the proteolysis of damaged or misfolded proteins. Because it plays critical roles in the regulation of infectivity and virulence of many bacterial pathogens and is involved in various human diseases, interfering with ClpP activity has been evaluated as a potential

therapeutic strategy in the treatment of different ailments[32]. In-depth understanding of the mechanism of ClpP reaction and regulation is crucial for development of chemotherapeutic agents that target this protein. The importance of the dynamic equatorial region in ClpP has long been recognized[21-24, 29-31].

As the first identified inhibitor targeting flexible handle region of ClpP, cediranib shows a distinct inhibitory mechanism. The cediranib-bound *Mtb*ClpP1P2 complex structure provides valuable evidence to support the important roles of equatorial handle domain for ClpP function[21][26]. Compared with the highly conserved critical residues in the N-terminal region of α5 (Ile136, Ile138, and Ala140 in *Mtb*ClpP1) (Fig 4C), residues participating in cediranib binding are relatively diverse among different ClpP homologs, leading to a substantial variation in the size of the binding pockets near to the side pores, which suggests this mechanism could be employed for pathogen-selective ClpP inhibitor development.

Materials and Methods

Bacterial strains and culture conditions. *Escherichia coli* DH5α and BL21 (DE3) were cultured at 37℃ in Luria broth (LB) and LB-agar plates. DNA encoding *M. tuberculosis* ClpP1 and ClpP2 (spanning residues 7–200 and 13–214, respectively) was cloned into a pRSF-Duet vector preceded by an N-terminal His_6-SUMO tag (Novagen)[11, 12]. Full-length *Ec*ClpP, *Sa*ClpP, *Pa*ClpP1 and the *h*ClpP gene without its mitochondrial targeting sequence (residues Met1–Pro57) were also respectively cloned into pRSF-Duet preceded by an N-terminal His_6-SUMO tag[33-35]. PCR was performed with PrimeSTAR® max DNA polymerase (Takara) and *Ex Taq*® polymerase

(Takara). The plasmids carrying distinct ClpP genes were transformed into *Escherichia coli* BL21 (DE3) cells (TransGen Biotech). The plasmids and primers used in this study are listed in Appendix Table S1 and Appendix Table S2.

Protein expression and purification. *M. tuberculosis* ClpP1 (residues 7–200) and ClpP2 (residues 13–214) with N-terminal His_6-SUMO tags were expressed and purified as described, with minor modifications[11, 12, 14]. In short, ClpP1 and ClpP2 were individually overexpressed in *E. coli* strain BL21 (DE3) in LB broth at 16 ℃, following induction with 0.5 mM isopropyl β-D-1-thiogalactopyranoside for about 16 h with shaking at 220 rpm in medium supplemented with 50 μg/mL kanamycin. Cells were resuspended and lysed in buffer containing 50 mM K_2HPO_4/KH_2PO_4, pH 7.6, 500 mM KCl, 10% glycerol and 0.5 mM dithiothreitol. His-tagged *Mtb*ClpP1/*Mtb*ClpP2 proteins were purified using a nickel affinity column and eluted with the same buffer supplemented with 250 mM imidazole. The His_6-SUMO tag of eluted proteins was removed using ubiquitin-like-protease 1 (ULP1) at 4 ℃. The tag-free proteins were further purified by anion exchange chromatography (MonoQ; GE Healthcare). Peak fractions were collected, concentrated and applied to Superdex 200 16/600 (GE Healthcare) preequilibrated with buffer containing 10 mM HEPES, pH 7.5, 50 mM NaCl and 2 mM dithiothreitol for final purification. Purified ClpP1 and ClpP2 were concentrated in Amicon centrifugal concentration devices (Millipore) to >80 μM tetradecamer. *Ec*ClpP, *Sa*ClpP, *Pa*ClpP1 and *h*ClpP proteins were expressed as described above. These proteins were purified using a nickel affinity column and then incubated with ULP1 at 4 ℃ to cleave the His_6-SUMO tag[36].

Compound screening. The peptidase activity of *Mtb*ClpP1P2 was monitored at 30 ℃ in black 96-well plates, as described[11, 14]. After peptide bond cleavage, the fluorophore 7-amino-4-methylcoumarin of the fluorogenic substrate Z-Gly-Gly-Leu-AMC is liberated and can be quantified. Briefly, each well contained 100 μM fluorogenic peptide, 0.5 μM tetradecamer ClpP1P2, and 2 mM Bz-LL in 80 μL of buffer containing 50 mM phosphate buffer, pH 7.6, 300 mM KCl, 5 mM $MgCl_2$ and 5% glycerol. Substrate cleavage was monitored using an all-in-one microplate reader (Gen5; BioTek) by exciting at 380 nm and following the increase in fluorescence emission at 460 nm. The deviation of fluorescence value in at least two independent measurements was ≤5%. The screening assay was carried out in 96-well format as described above, and about 2600 compounds were screened at 100 μM. Positive (bortezomib) and negative controls (dimethyl sulfoxide; DMSO) were included on every plate and were used to assess the performance of the primary screen. Bz-LL was purchased from GL Biochem (Shanghai) Ltd. Cediranib was purchased from MedChemExpress.

IC_{50} determination. To determine the potency of the 8 "hit" compounds against *Mtb*ClpP1P2, these compounds were tested at concentrations ranging from 1 to 100 μM in a 96-well plate format. The reaction mix contained 0.5 μM *Mtb*ClpP1P2 tetradecamer and 2 mM Bz-LL, with 0.8 μL of each dilution of the compound or DMSO in a total volume of 80 μL. The reaction was initiated by addition of 0.8 μL of 10 mM fluorogenic substrate Z-Gly-Gly-Leu-AMC (100 μM final concentration) to the reaction mix. Initial velocity data was obtained by the monitoring increase in the fluorescence due to hydrolysis of the substrate using the microplate reader at 10-min

intervals over 60 min. The IC_{50} value for each compound was obtained by nonlinear regression curve fitting of a four-parameter variable slope equation to the dose–response data using Prism software.

The peptidase activity of *Ec*ClpP, *Sa*ClpP, *Pa*ClpP1 and *h*ClpP was determined using a fluorescence-based assay with Suc-LY-AMC as the substrate, according to literature protocols[33-35]. The reaction mix contained 0.5 μM *Ec*ClpP/2.5 μM *Sa*ClpP/0.5 μM *Pa*ClpP/3 μM *h*ClpP tetradecamer, with 0.8 μL of each dilution of the test compound or DMSO in a total volume of 80 μL. The IC_{50} values for cediranib against *Ec*ClpP, *Sa*ClpP, *Pa*ClpP1 and *h*ClpP were obtained as described above.

Non-competitive inhibition was investigated by using 0.5 μM *Mtb*ClpP1P2 tetradecamer and 2 mM Bz-LL with different concentrations of cediranib. An equivalent volume of DMSO was added to the control group. The serially diluted substrate (500, 400, 300, 200, 100 and 50 μM) was added into wells of a 96-well plate and incubated for 30min at room temperature. Fluorescence was measured at 30 ℃ using the microplate reader (excitation, 380 nm; emission, 460 nm) for 1 h[9].

Crystallization. Cediranib-*Mtb*ClpP1P2 complex crystals were prepared by the hanging drop method referring to previously published works[12, 19]. The precipitant solution consisted of 1.5 M $(NH_4)_2SO_4$ and 0.1 M MES, pH 6.5. A drop contained a mixture of 2 μL protein (about 2.5 mg/mL ClpP1 and ClpP2, 0.2 mM cediranib maleate, 5 mM Bz-LL, 10 mM HEPES, 50 mM NaCl, 2 mM DTT, pH 7.5) and 2 μL of precipitant solution and was incubated at 18 ℃ for about 3 months. Crystals were soaked briefly in 2 M Li_2SO_4 solution and were stored in liquid nitrogen.

Data collection and structure determination. The X-ray data were collected with a CCD camera at station BL-19U of the Shanghai synchrotron radiation facility (SSRF), Shanghai, China. The diffraction data were indexed, integrated, and scaled using the HKL2000 program suite[37]. The process of structure building and refinement was monitored using the COOT and PHENIX suites[38, 39]. The PDB code for the co-crystal structure of cediranib with *Mtb*ClpP1P2 (resolution 2.7 Å) is 6IW7.

DSC. DSC-based analysis of the thermal denaturation of proteins provides an approach for measuring protein–ligand interactions[40]. Samples for DSC were prepared following the operating manual of the instrument. *Mtb*ClpP1P2 was dissolved to a final concentration of 0.5 mg/mL. The molar ratio between *Mtb*ClpP1P2 and compounds was 10:1 in reaction cells. DSC measurements were performed using a VP-DSC Micro Calorimeter (Microcal, USA) at a scan rate of 0.5–2 ℃/min in the temperature range 10–110 ℃. Six-pair blank cells with buffer (50 mM phosphate buffer, pH 7.6, 300 mM KCl, 5 mM $MgCl_2$ and 5% glycerol, with the same volume of DMSO) were prepared to obtain instrumental baselines, which were systematically subtracted from the sample experimental thermograms. A thermal transition curve was obtained from a plot of heat capacity against temperature.

Mutagenesis. Thirty-one mutations were introduced by site-directed mutagenesis, primers are listed in Appendix Table S3. The PCR products were extracted with PCR purification kits (Takara 9761) and ligated using a Blunting Kination Ligation Kit (Takara 6217). The mutated sequences of the ClpP1 gene were confirmed by DNA sequencing (Tsingke). Variant ClpP1 proteins were expressed in *Escherichia coli* BL21

(DE3) for enzymatic cleavage assays. The IC_{50} values of cediranib toward *Mtb*ClpP1P2 mutants were determined in the same way as that for wild-type *Mtb*ClpP1P2.

Molecular Dynamics Simulations. The molecular dynamics simulations were performed in AMBER 14 software package[41]. The initial coordinates for molecular dynamics simulation were firstly prepared through structural inspection and optimization in Schrödinger software suite[42]. In the tleap module of AMBER, *Mtb*ClpP1P2 dimer was solvated in a rectangular water box of TIP3P and neutralized with Na+ ions. The periodic boundary conditions were setup with all the solvents 10 Å away from the solutes. The protein were parameterized using the AMBER FF99SB force field[43] and the ligands were parameterized using the GAFF force filed[44]. Energy minimization was performed firstly to remove the local atomic collision in the systems and the combination of the descent steepest with conjugated gradient method was adopted in the process. In the NVT ensemble, the systems were heated from 0 to 310 K gradually and the solutes were restrained with harmonic force constant 5 kcal/mol/Å2 simultaneously. Five equilibration stages were performed to adjust the solvents density. Finally, 500ns conventional molecular dynamics (cMD) simulations were performed in the NPT ensemble, with coordinates saved every 5 ps throughout the entire process.

Data analysis for MD simulation. Root-mean-square deviation (RMSD) for the proteins and ligands during the simulations were calculated using the CPPTRAJ module[45] of AmberTools 13 package[41] to characterize the conformational change of the proteins and ligands. Standardized secondary structures assignment analysis were

calculated with the DSSP algorithm using the AmberTools 13 package, which can characterize the propensities of secondary structures for each residue during the simulations. Then the heatmap for DSSP analysis was plotted using the MATLAB package (MathWorks, USA).Principal Component Analysis (PCA) analysis on the basis of covariance matrix was carried out using the program Carma[46] to address the collective motions of *Mtb*ClpP1P2. A two-dimensional representation of Free Energy Landscape (FEL) was built based on the PCA analysis, and two dominant components of PC1 and PC2 were selected as the reaction coordinates. The FEL along the reaction coordinates could be calculated using the following equation[47]:

$$\Delta G(PC1, PC2) = -\kappa_B T \ln g(PC1, PC2)$$

where T and κB represent the temperature of MD simulations and the Boltzmann constant, respectively. The g(PC1,PC2) is the normalized joint probability. Then the structures for the lowest energy in FEL were extracted as the representative conformation of each energy basin. These representative structures were superimposed to the initial crystal structure for comparison.

Acknowledgements

We would like to thank Professor Jikui Song for generously sharing the plasmids used to generate ClpPs proteins. X-ray diffraction image collection, analysis and computation work were performed using the workstations at Shanghai Synchrotron Radiation Facility.

Author contributions

Conceptualization: Youfu Luo.

Data curation: Yang Yang, Yibo Zhu and Huanxiang Liu.

Formal analysis: Yang Yang, Yibo Zhu,Tao Yang, Tao Li, Yuan Ju, Yingjie Song, Huanxiang Liu, Jun He, Rui Bao and Youfu Luo.

Funding acquisition: Rui Bao and Youfu Luo.

Investigation: Yang Yang,Yibo Zhu,Tao Yang,Tao Li, Yuan Ju, Yingjie Song, Jun He and Huanxiang Liu.

Resources: Rui Bao and Youfu Luo.

Supervision: Tao Yang, Rui Bao and Youfu Luo.

Validation: Yang Yang, Yibo Zhu, Tao Yang, Rui Bao and Youfu Luo.

Visualization: Yang Yang, Yibo Zhu and Rui Bao.

Writing-original draft: Yang Yang, Yibo Zhu,Tao Yang, Rui Bao and Youfu Luo.

Writing-review & editing: Yang Yang, Rui Bao and Youfu Luo.

Competing interests

The authors declare no competing interests.

References

1. Olivares AO, Baker TA, Sauer RT. Mechanistic insights into bacterial AAA+ proteases and protein-remodelling machines. Nat Rev Microbiol. 2016;14(1):33-44. https://doi:10.1038/nrmicro.2015.4 PMID:26639779.
2. Bhandari V, Wong KS, Zhou JL, Mabanglo MF, Batey RA, Houry WA. The Role of ClpP Protease in Bacterial Pathogenesis and Human Diseases. ACS Chem Biol. 2018;13(6):1413-25. https://doi:10.1021/acschembio.8b00124 PMID:29775273.
3. Sassetti CM, Boyd DH, Rubin EJ. Genes required for mycobacterial growth defined by high density mutagenesis. Mol Microbiol. 2003;48(1):77-84. https://doi:10.1046/j.13652958.2003.03425.x PMID:12657046.
4. Brötz-Oesterhelt H, Beyer D, Kroll H-P, Endermann R, Ladel C, Schroeder W, et al. Dysregulation of bacterial proteolytic machinery by a new class of antibiotics. Nat Med. 2005;11(10):1082-7. https://doi:10.1038/nm1306 PMID: 16200071
5. Conlon BP, Nakayasu ES, Fleck LE, LaFleur MD, Isabella VM, Coleman K, et al. Activated ClpP kills persisters and eradicates a chronic biofilm infection. Nature. 2013;503(7476):365-70.

https://doi:10.1038/nature12790 PMID:24226776.

6. Moreno-Cinos C, Sassetti E, Salado IG, Witt G, Benramdane S, Reinhardt L, et al. alpha-Amino Diphenyl Phosphonates as Novel Inhibitors of Escherichia coli ClpP Protease. J Med Chem. 2019;62(2):774-97. https://doi:10.1021/acs.jmedchem.8b01466 PMID:30571121.

7. Fraga H, Rodriguez B, Bardera A, Cid C, Akopian T, Kandror O, et al. Development of high throughput screening methods for inhibitors of ClpC1P1P2 from Mycobacteria tuberculosis. Anal Biochem. 2019;567:30-7. https://doi:10.1016/j.ab.2018.12.004.

8. Markus Lakemeyer EB, Friederike Möller, Dóra, Balogh RS, Hendrik Dietz, Stephan Axel, Sieber. Tailored Peptide Phenyl Esters Block ClpXP Proteolysis by an Unusual Breakdown into a Heptamer–Hexamer Assembly. Angew Chem Int Ed. 2019;58:1-7. https://doi:10.1002/anie.201901056 PMID: 30829431

9. Vahidi S, Ripstein ZA, Bonomi M, Yuwen T, Mabanglo MF, Juravsky JB, et al. Reversible inhibition of the ClpP protease via an N-terminal conformational switch. Proc Natl Acad Sci U S A. 2018;115(28):E6447-E56. https://doi:10.1073/pnas.1805125115 PMID: 29941580

10. Ollinger J, O'Malley T, Kesicki EA, Odingo J, Parish T. Validation of the Essential ClpP Protease in Mycobacterium tuberculosis as a Novel Drug Target. J Bacteriol. 2012;194(3):663-8.

11. Akopian T, Kandror O, Raju RM, Unnikrishnan M, Rubin EJ, Goldberg AL. The active ClpP protease from M. tuberculosis is a complex composed of a heptameric ClpP1 and a ClpP2 ring. EMBO J. 2012;31(6):1529-41. https://doi:10.1038/emboj.2012.5 PMID:22286948.

12. Schmitz KR, Carney DW, Sello JK, Sauer RT. Crystal structure of Mycobacterium tuberculosis ClpP1P2 suggests a model for peptidase activation by AAA+ partner binding and substrate delivery. Proc Natl Acad Sci U S A. 2014;111(43):E4587-95. https://doi:10.1073/pnas.141712-0111 PMID:25267638.

13. Raju RM, Unnikrishnan M, Rubin DH, Krishnamoorthy V, Kandror O, Akopian TN, et al. Mycobacterium tuberculosis ClpP1 and ClpP2 function together in protein degradation and are required for viability in vitro and during infection. PLoS Pathog. 2012;8(2):e1002511. https://doi:10.1371/journal.ppat.1002511 PMID: 22359499

14. Compton CL, Schmitz KR, Sauer RT, Sello JK. Antibacterial activity of and resistance to small molecule inhibitors of the ClpP peptidase. ACS Chem Biol. 2013;8(12):2669-77. https://doi:10.1021/cb400577b PMID:24047344.

15. Akopian T, Kandror O, Tsu C, Lai JH, Wu W, Liu Y, et al. Cleavage Specificity of Mycobacterium tuberculosis ClpP1P2 Protease and Identification of Novel Peptide Substrates and Boronate Inhibitors with Anti-bacterial Activity. J Biol Chem. 2015;290(17):11008-20. https://doi:10.1074/jbc.M114.625640 PMID:25759383.

16. Moreira W, Ngan GJ, Low JL, Poulsen A, Chia BC, Ang MJ, et al. Target mechanism-based whole-cell screening identifies bortezomib as an inhibitor of caseinolytic protease in mycobacteria. mBio. 2015;6(3):e00253-15. https://doi:10.1128/mBio.00253-15 PMID:25944-857.

17. Moreira W, Santhanakrishnan S, Ngan GJY, Low CB, Sangthongpitag K, Poulsen A, et al. Towards Selective Mycobacterial ClpP1P2 Inhibitors with Reduced Activity against the Human Proteasome. Antimicrob Agents Chemother. 2017;61(5). https://doi:10.1128/AAC.02307-16 PMID:28193668.

18. Lee BG, Park EY, Lee KE, Jeon H, Sung KH, Paulsen H, et al. Structures of ClpP in complex

with acyldepsipeptide antibiotics reveal its activation mechanism. Nat Struct Mol Biol. 2010;17(4):471-8. https://doi:10.1038/nsmb.1787 PMID:20305655.

19. Li M, Kandror O, Akopian T, Dharkar P, Wlodawer A, Maurizi MR, et al. Structure and Functional Properties of the Active Form of the Proteolytic Complex, ClpP1P2, from Mycobacterium tuberculosis. J Biol Chem. 2016;291(14):7465-76. https://doi:10.1074/jbc.M115.700344 PMID:26858247.

20. Ingvarsson H, Mate MJ, Hogbom M, Portnoi D, Benaroudj N, Alzari PM, et al. Insights into the inter-ring plasticity of caseinolytic proteases from the X-ray structure of Mycobacterium tuberculosis ClpP1. Acta Crystallogr D Biol Crystallogr. 2007;63(Pt 2):249-59. https://doi:10.1107/S0907444906050530 PMID:17242518.

21. Sprangers R, Gribun A, Hwang PM, Houry WA, Kay LE. Quantitative NMR spectroscopy of supramolecular complexes: dynamic side pores in ClpP are important for product release. Proc Natl Acad Sci U S A. 2005;102(46):16678-83. https://doi:10.1073/pnas.0507370102 PMID:16263929.

22. Gribun A, Kimber MS, Ching R, Sprangers R, Fiebig KM, Houry WA. The ClpP double ring tetradecameric protease exhibits plastic ring-ring interactions, and the N termini of its subunits form flexible loops that are essential for ClpXP and ClpAP complex formation. J Biol Chem. 2005;280(16):16185-96. https://doi:10.1074/jbc.M414124200 PMID:15701650.

23. Zhang J, Ye F, Lan L, Jiang H, Luo C, Yang CG. Structural switching of Staphylococcus aureus Clp protease: a key to understanding protease dynamics. J Biol Chem. 2011;286(43):37590-601. https://doi:10.1074/jbc.M111.277848 PMID:21900233.

24. Ye F, Zhang J, Liu H, Hilgenfeld R, Zhang R, Kong X, et al. Helix unfolding/refolding characterizes the functional dynamics of Staphylococcus aureus Clp protease. J Biol Chem. 2013;288(24):17643-53. https://doi:10.1074/jbc.M113.452714 PMID:23625918.

25. Gersch M, Kolb R, Alte F, Groll M, Sieber SA. Disruption of oligomerization and dehydroalanine formation as mechanisms for ClpP protease inhibition. J Am Chem Soc. 2014;136(4):1360-6. https://doi:10.1021/ja4082793 PMID:24106749.

26. Personne Y, Brown AC, Schuessler DL, Parish T. Mycobacterium tuberculosis ClpP Proteases Are Co-transcribed but Exhibit Different Substrate Specificities. PLoS One. 2013;8(4):e60228. https://doi:10.1371/journal.pone.0060228 PMID:23560081

27. Szyk A, Maurizi MR. Crystal structure at 1.9A of E. coli ClpP with a peptide covalently bound at the active site. J Struct Biol. 2006;156(1):165-74. https://doi:10.1016/j.jsb.2006.03.013 PMID:16682229.

28. Mundra S, Thakur V, Bello AM, Rathore S, Asad M, Wei L, et al. A novel class of Plasmodial ClpP protease inhibitors as potential antimalarial agents. Bioorg Med Chem. 2017;25(20):5662-77. https://doi:10.1016/j.bmc.2017.08.049 PMID:28917450.

29. Liu K, Ologbenla A, Houry WA. Dynamics of the ClpP serine protease: a model for self-compartmentalized proteases. Crit Rev Biochem Mol Biol. 2014;49(5):400-12. https://doi:10.3109/10409238.2014.925421 PMID:24915503.

30. Lee BG, Kim MK, Song HK. Structural insights into the conformational diversity of ClpP from Bacillus subtilis. Molecules and cells. 2011;32(6):589-95. https://doi:10.1007/s10059-011-0197-1 PMID:22080375.

31. Geiger SR, Bottcher T, Sieber SA, Cramer P. A conformational switch underlies ClpP protease function. Angew Chem Int Ed. 2011;50(25):5749-52. https://doi:10.1002/anie.201100666

PMID:21544912.

32. Dougan DA, Hantke I, Turgay K. Dysregulating ClpP: From Antibiotics to Anticancer? Cell Chem Biol. 2018;25(8):929-30. https://doi:10.1016/j.chembiol.2018.08.002 PMID:30118671.

33. Hackl MW, Lakemeyer M, Dahmen M, Glaser M, Pahl A, Lorenz-Baath K, et al. Phenyl Esters Are Potent Inhibitors of Caseinolytic Protease P and Reveal a Stereogenic Switch for Deoligomerization. J Am Chem Soc. 2015;137(26):8475-83. https://doi:10.1021/jacs.5b03084 PMID:26083639.

34. Hall BM, Breidenstein EBM, de la Fuente-Nunez C, Reffuveille F, Mawla GD, Hancock REW, et al. Two Isoforms of Clp Peptidase in Pseudomonas aeruginosa Control Distinct Aspects of Cellular Physiology. J Bacteriol. 2017;199(3). https://doi:10.1128/JB.00568-16 PMID:2784-9175.

35. Gronauer TF, Mandl MM, Lakemeyer M, Hackl MW, Messner M, Korotkov VS, et al. Design and synthesis of tailored human caseinolytic protease P inhibitors. Chem Commun (Camb). 2018;54(70):9833-6. https://doi:10.1039/c8cc05265d PMID:30109319.

36. Zhang Z-M, Ma K-W, Yuan S, Luo Y, Jiang S, Hawara E, et al. Structure of a pathogen effector reveals the enzymatic mechanism of a novel acetyltransferase family. Nat Struct Mol Biol. 2016;23(9):847-52. https://doi:10.1038/nsmb.3279 PMID:27525589.

37. Z O, W M. Processing of X-ray diffraction data collected in oscillation mode. Methods Enzymol. 1997;276(97):307-26 PMID:27754618.

38. Adams PD, Afonine PV, Bunkoczi G, Chen VB, Davis IW, Echols N, et al. PHENIX: a comprehensive Python-based system for macromolecular structure solution. Acta Crystallogr D Biol Crystallogr. 2010;66(Pt 2):213-21. https://doi:10.1107/S0907444909052925 PMID:2012-4702.

39. Emsley P, Lohkamp B, Scott WG, Cowtan K. Features and development of Coot. Acta Crystallogr D Biol Crystallogr. 2010;66(Pt 4):486-501. https://doi:10.1107/S090744491007493 PMID:20383002.

40. Holdgate GA, Ward WHJ. Measurements of binding thermodynamics in drug discovery. Drug Discov Today. 2005;10(22):1543-50. https://doi:10.1016/s1359-6446(05)03610-x PMID: 16257377

41. D. A. Case TAD, T. E. Cheatham III, C. L.Simmerling, J. Wang, R. L. R. E. Duke, W. Z. R. C. Walker, K. M. Merz, B. Roberts, S. Hayik, A. Roitberg, J. S. G. Seabra, I. K. A. W. Goetz, F. P. K. F. Wong, J. Vanicek, R. M. Wolf, J. Liu, S. R. B. X. Wu, T. Steinbrecher, H. Gohlke, Q. Cai, X. Ye, J. Wang, M.-J. Hsieh, G. Cui, D. R. Roe, D. H. Mathews, M. G. Seetin, R. Salomon-Ferrer, C. Sagui, V. Babin, T. Luchko, S. Gusarov, A. Kovalenko and P. A. Kollman. Amber 14. San Francisco: University of California; 2014.

42. Schrödinger L. The PyMOL molecular graphics system, version 1.8. New York: ; 2015.

43. Hornak V, Abel R, Okur A, Strockbine B, Roitberg A, Simmerling C. Comparison of multiple Amber force fields and development of improved protein backbone parameters. Proteins. 2006;65(3):712-25. https://doi:10.1002/prot.21123 PMID:16981200.

44. Roe DR, Cheatham TE, 3rd. PTRAJ and CPPTRAJ: Software for Processing and Analysis of Molecular Dynamics Trajectory Data. Journal of chemical theory and computation. 2013;9(7):3084-95. https://doi:10.1021/ct400341p PMID:26583988.

45. Junmei Wang, Main M. Wolf, James W, Caldwell, Peter A. Kollman, Case. DA. Development and Testing of a General Amber Force Field. J Comput Chem. 2004;25(9):1157-74.

https://doi:10.1002/jcc.20035 PMID:15116359.

46. Glykos NM. Software news and updates. Carma: a molecular dynamics analysis program. J Comput Chem. 2006;27(14):1765-8. https://doi:10.1002/jcc.20482 PMID:16917862.

47. Papaleo E, Mereghetti P, Fantucci P, Grandori R, De Gioia L. Free-energy landscape, principal component analysis, and structural clustering to identify representative conformations from molecular dynamics simulations: the myoglobin case. J Mol Graph Model. 2009;27(8):889-99. https://doi:10.1016/j.jmgm.2009.01.006 PMID:19264523.

Figures legends

Fig 1. Cediranib inhibits *Mycobacterium tuberculosis* (*Mtb*) caseinolytic protease P1P2 (*Mtb*ClpP1P2) activity. (A) Chemical structure of compounds for secondary screening. (B) Cediranib inhibits *Mtb*ClpP1P2 cleavage of substrate Z-Gly-Gly-Leu-AMC in a peptidase assay. Concentrations of *Mtb*ClpP1P2 and Z-Gly-Gly-Leu-AMC were 0.5 μM and 100 μM, respectively. (C) Noncompetitive inhibition of *Mtb*ClpP1P2 cleavage of Z-Gly-Gly-Leu-AMC by cediranib. Cediranib increased the maximum reaction velocity (Vmax), but did not affect the Michaelis constant (Km) of the *Mtb*ClpP1P2 reaction.

Fig 2. Cediranib-bound ClpP1P2 structures. (A) Side view of the *Mtb*ClpP1P2 tetradecamer. The *Mtb*ClpP1 heptamer (cyan subunits) and *Mtb*ClpP2 heptamer (orange subunits) are shown in cartoon representation. Spheres represent cediranib molecules (green) bound to the *Mtb*ClpP1 ring and Bz-Leu-Leu (Bz-LL) peptide (yellow) bound to the active sites of both rings. (B) Top panel, axial view of the *Mtb*ClpP1P2 tetradecamer from the *Mtb*ClpP1 side; bottom panel, axial view of the *Mtb*ClpP1P2 tetradecamer from the *Mtb*ClpP2 side. (C) *Mtb*ClpP1P2 monomer magnified from cediranib-bound *Mtb*ClpP1P2 structure. Secondary structure elements are labeled. The *Mtb*ClpP1P2 handle region and the catalytic triad residues are labeled. Cediranib and Bz-LL are colored green and yellow, respectively.

Fig 3. Structural details of cediranib binding pocket in *Mtb*ClpP1. (A) The activator is bound in opposite orientations in *Mtb*ClpP1 and *Mtb*ClpP2. Bz-LL in *Mtb*ClpP1 is colored yellow and Bz-LL in *Mtb*ClpP2 is colored gray. (B) 2Fo−Fc electron-density map of cediranib in *Mtb*ClpP1. (C) Surface representation of the *Mtb*ClpP1P2 tetradecamer with bound cediranib reveals that cediranib binds in a novel site. (D) A cartoon representation of the cediranib interactions with *Mtb*ClpP1. (E) Molecular interactions between cediranib and residues in the binding pocket. Cediranib does not interact directly with the active site, but interferes with the presumably defined equatorial pores and dynamic handle regions. (F) Detailed view of the cediranib-bound

pocket formed by residues Gln142–Glu149 in α5, Ile71–Ala76 in α3, and three short β-sheets (βD, βF, βH) from the neighboring *Mtb*ClpP1 subunit.

Fig 4. Importance of the handle domain and analysis of distinct ClpP sequences. Importance of the handle domain and analysis of distinct ClpP sequences. (A) Superposition and ribbon representation of the monomeric structures of *Mtb*ClpP1 (cyan), *Mtb*ClpP2 (orange), Staphylococcus aureus (Sa)ClpP (green), Escherichia coli (Ec)ClpP (light blue), Listeria monocytogenes (Lm)ClpP1 (pink), LmClpP2 (magenta), and human (h)ClpP (gray). (B) *Mtb*ClpP1P2 side views. Mutant residue sites are labeled. Spheres represent cediranib molecules (green) bound to the *Mtb*ClpP1 ring and Bz-Leu-Leu (Bz-LL) peptide (yellow) bound to the active sites of both rings. (C) Sequence alignment and secondary structure assignment of ClpPs. Sequence alignment was performed in BioEdit. Identical residues are highlighted in blue. Secondary structure elements present in the *Mtb*ClpP1P2 structure (PDB code 6IW7) are shown on the top of the sequence alignment.

Supporting Information

S1 Table. Plasmids used in this study.

(DOCX)

S2 Table. Primers used in this study.

(DOCX)

S3 Table. Strains used in this study.

(DOCX)

S1 Fig. Differential scanning calorimetry analysis of the binding between cediranib and *Mtb*ClpP1P2. The concentrations of bortezomib and cediranib were 100 μM.

(TIF)

S2 Fig. Inhibition of cediranib aganist *Ec*ClpP, *Sa*ClpP, *Pa*ClpP and *h*ClpP.

(A) Inhibition of cediranib on *Ec*ClpP. Concentration of *Ec*ClpP was 0.5μM. (B) Inhibition of cediranib on *Sa*ClpP. Concentration of *Sa*ClpP was 2.5 μM. (C) Inhibition of cediranib on *Pa*ClpP. Concentration of *Pa*ClpP was 0.5 μM. (D) IC_{50} value of cediranib aganist *h*ClpP. Concentration of *h*ClpP was 2.5μM.

(TIF)

S3 Fig. Conformational changes of *Mtb*ClpP1 dimer.

(A,C). Cα RMSD values of the head domain and handle domain in *Mtb*ClpP1 dimer versus simulation time without (A)or with cediranib(C). The RMSD values of the head domain and handle domain are shown in green and red, respectively. (B,D). Secondary structures as a function of time for *Mtb*ClpP1 dimer without (B)or with cediranib(D) in

604 trajectory as calculated using DSSP. The structures were analyzed every 100 ps. (E,F).
605 Left, energy landscape for the conformational transition of *Mtb*ClpP1 dimer without
606 (E)or with cediranib(F). Reaction coordinates were defined according to PC1 and PC2
607 obtained from PCA. Right,snapshot structures of α5 from *Mtb*ClpP1 dimer without
608 (E)or with cediranib(F) extracted from the trajectory.
609 (TIF)
610

611 **Table 1. Minimum inhibitory concentrations (MIC) against different bacterial**
612 **strains and the inhibition of ClpP peptidase activity by cediranib.**

Organism	MIC （μg/mL）	IC_{50}（μM）	Selectivity Index[b]
M. tuberculosis H37Rv	16	3.4±0.7	/
M. smegmatis MC^2155	64	NT[a]	NT
E. coli	>128	>100	>30
S. aureus	>128	>100	>30
P. aeruginosa	>128	>100	>30
Homo sapiens	/	36.6±0.5	10.8

613 [a] NT, not tested. [b] Selectivity Index calculated as Cediranib IC_{50} of ClpPs / cediranib
614 IC_{50} of *Mtb*ClpP1P2.

615

616 **Table 2. Minimum inhibitory concentration of cediranib against different strains.**

Strains		Cediranib (μg/mL)	Linezolid (μg/mL)	Rifampin (μg/mL)	Bortezomib (μg/mL)
Escherichia coli	ATCC25922	>128	>128	4	>128
	ATCC35218	>128	>128	4	>128
Staphylococcus aureus	ATCC33591	>128	2	0.06	>128
	ATCC25923	>128	2	0.06	>128
Staphylococcus epidermidis	B27	64	1	0.06	>128
	ATCC12228	64	1	0.06	>128
Enterococcus faecalis	ATCC33186	>128	2	4	>128
Enterococcus faecium	ATCC35667	128	2	16	>128
Pseudomonas aeruginosa	ATCC27853	>128	>128	32	>128
	C58	>128	>128	32	>128
Klebsiella pneumoniae	ATCC4352	64	32	8	>128
	ATCC700603	>128	>128	32	>128

617 **Overall structure of cediranib-bound *Mtb*ClpP1P2**

618

619 **Table 3. Data collection and refinement statistics.**

Parameters	*Mtb*ClpP1P2 Cediranib-Bz-LL
Data collection	
Space group	*C*121
a, b, c(Å)	210.63 180.78 95.93
α, β, γ(°)	90.00 95.72 90.00
Wavelength(Å)	0.97915
Resolution(Å)	40.00 - 2.69(2.69 - 2.60)
$CC_{1/2}$	0.986(0.376)
Unique reflections	96900(9595)
R_{meas}(%)[a]	20.8(134)
Mean $I/\sigma(I)$[a]	8.04(1.04)
Completeness(%)[a]	98.6(98.2)
Redundancy	4.9(4.1)
Refinement	
Resolution(Å)	39.84 – 2.69
R_{work}/R_{free}[b]	0.2002/0.2433
No.atoms	
Protein	19747
Cediranib	413
Z-LL	350
Water	187
β-factors	
Protein	49.86
Cediranib	68.36
Z-LL	55.26
Water	48.67
R.m.s. deviations	
Bond lengths(Å)	0.009
Bond angles(°)	1.097
Ramachandran plot	
Favored (%)	97.08
Allowed (%)	2.73
Outliers (%)	0.19

620 [a] The values in parentheses are for the outermost shell.

621 [b] R_{free} is the R_{work} based on 5% of the data excluded from the refinement.

622 $R_{meas} = \sum_{hkl}\sqrt{n/(n-1)}\sum_{i=1}^{n}|I_i(hkl) - \langle I(hkl)\rangle| / \sum_{hkl}\sum_i I_i(hkl)$, where $\langle I(hkl)\rangle$

623 is the mean intensity of a set of equivalent reflections.

624 $R_{work} = \sum_{hkl}||F_{obs}| - |F_{calc}|| / \sum_{hkl} |F_{obs}|$, where F_{obs} and F_{calc} are observed and

625 calculated structure factors, respectively.

626 **Table 4. Mutagenesis analysis of *Mtb*ClpP1.**

Mutant	Activity	IC_{50}（μM）	Cediranib inhibition
/	+++++[a]	3.4±0.7	C[c]
I71F	–[b]		
I71V	+/–	>54.5	R[d]
S72T	+	NT[e]	
M75A	–		
M75F	–		
M75L	+	NT	
M75D	N/A[f]		
M95A	–		
M95Q	++++++++	23.7±0.7	R
M95L	++++	7.5±0.9	C
M95W	–		
M95S	+/–	>50	R
R119E	–		
R119Q	+	42.2±0.7	R
R119S	++	14.4±0.7	C
Q142H	+++	9.5±0.7	C
Q142R	–		
I146M	–		
I146V	+	5.1±0.7	C
I146T	+	9.7±1.3	C
I146L	–		
E149L	++++	41.8±0.9	R
E149R	+	>100	R
E149K	+	6.3±0.7	C
E149Q	++++++	7.6±0.9	C
E149 T	+++	12.8±0.8	C
W174I	–		
W174F	+/–	20.2±0.7	R
W174A	–		

627 [a] +, Having enzyme activity (the more plus signs, the higher the activity); [b] –, No
628 enzyme activity; [c] C, similar to wild-type *Mtb*ClpP1 (the control); [d] R, more resistant
629 than wild-type *Mtb*ClpP1 (R is defined as IC_{50} value of mutant protein/IC_{50} value of
630 wild-type protein >5); [e] NT, not tested; [f] N/A, protein unstable.

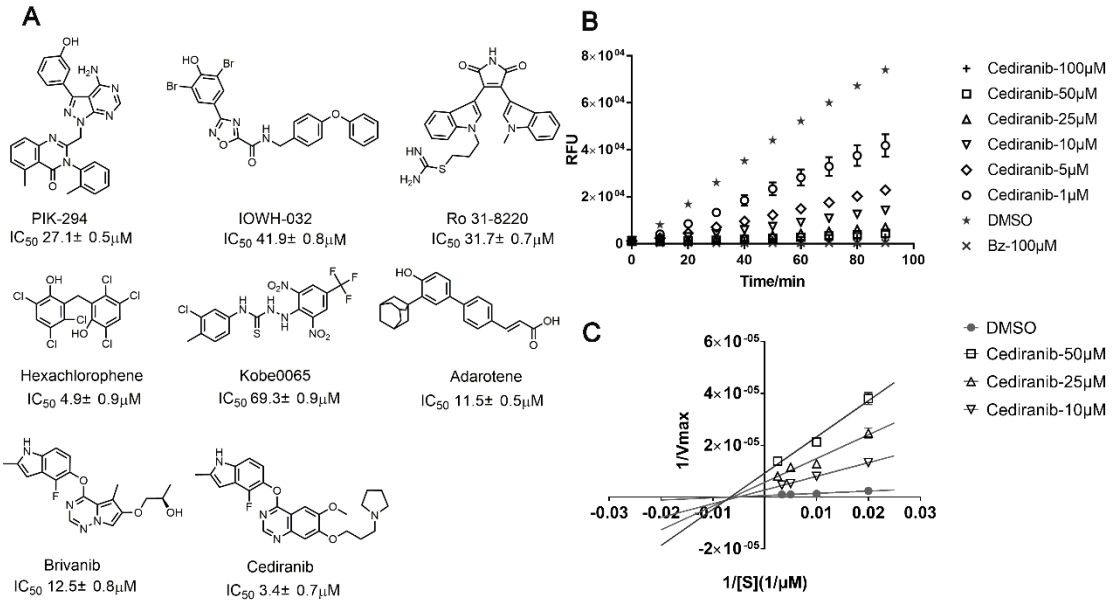

631

632 **Figure 1**

633

634

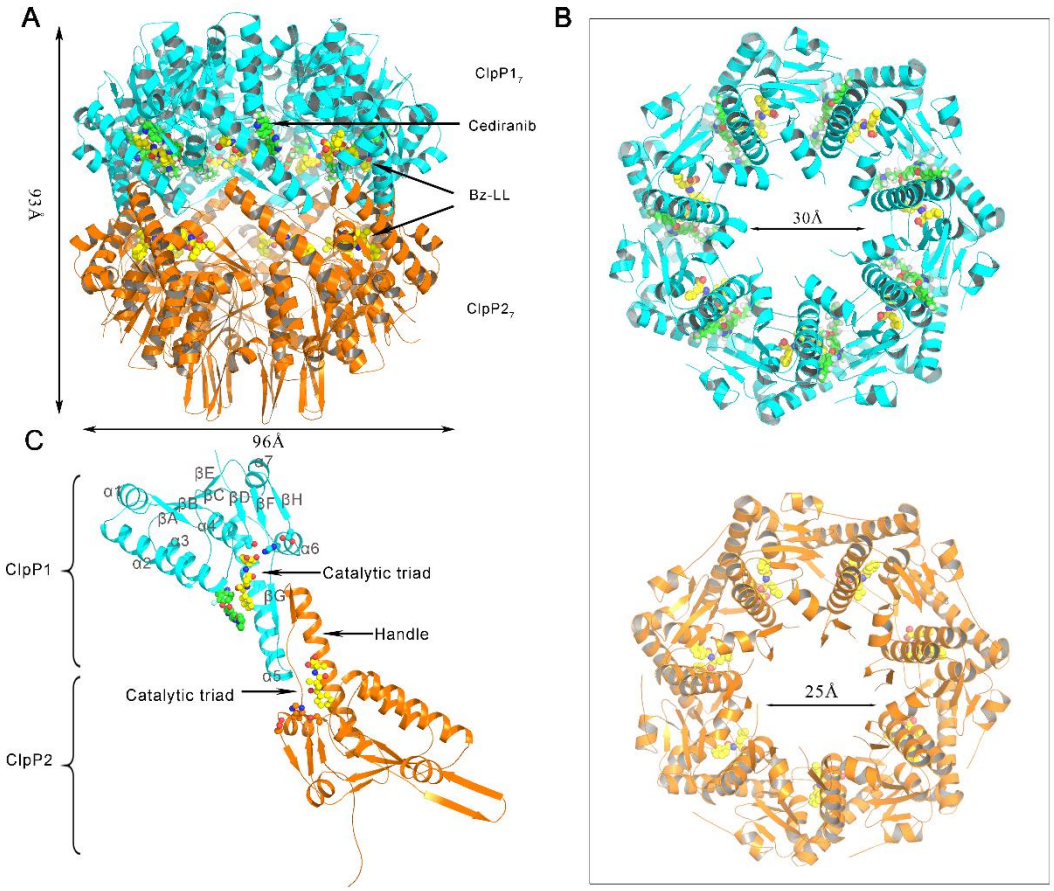

635

636 **Figure 2**

637

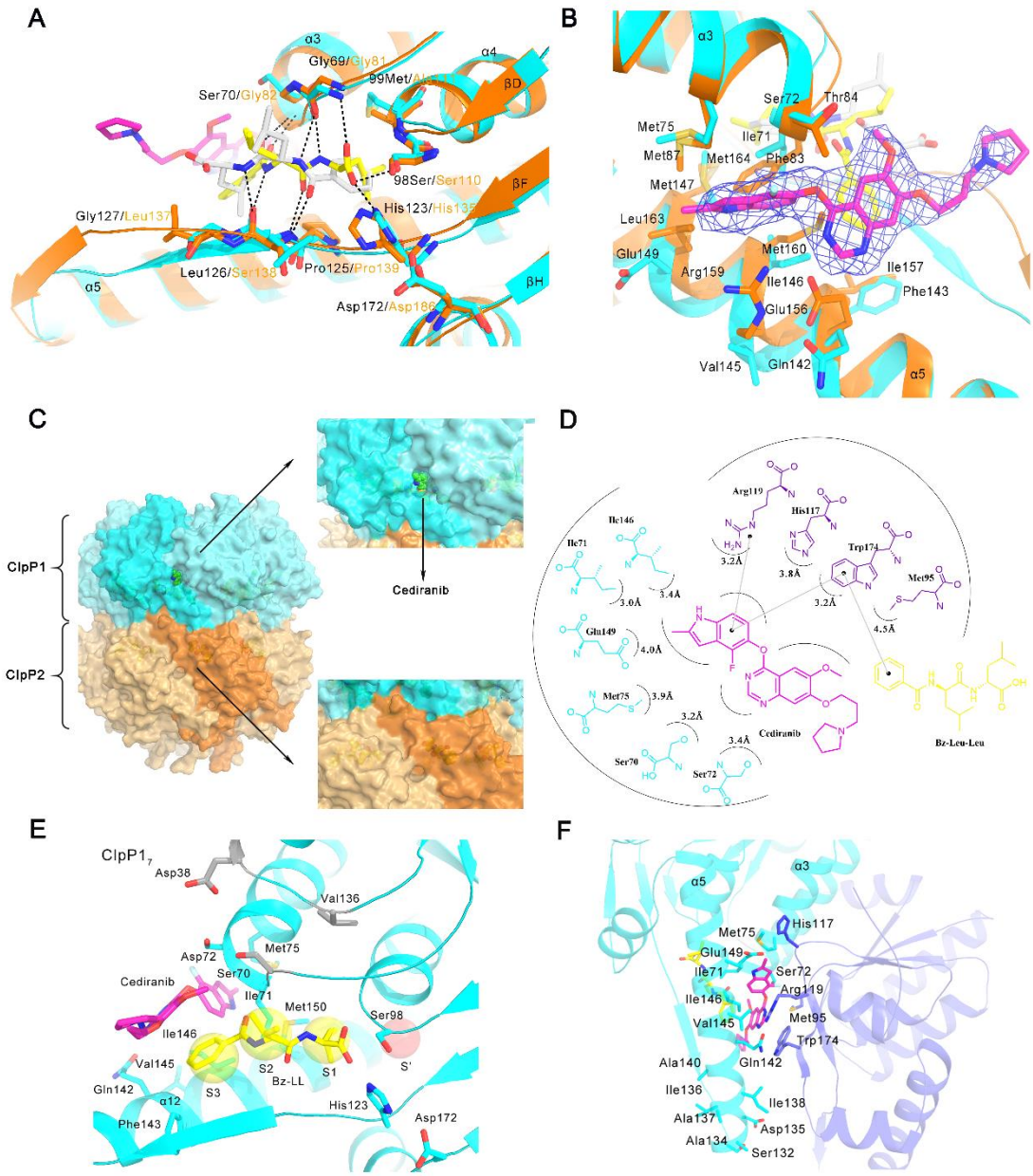

Figure 3

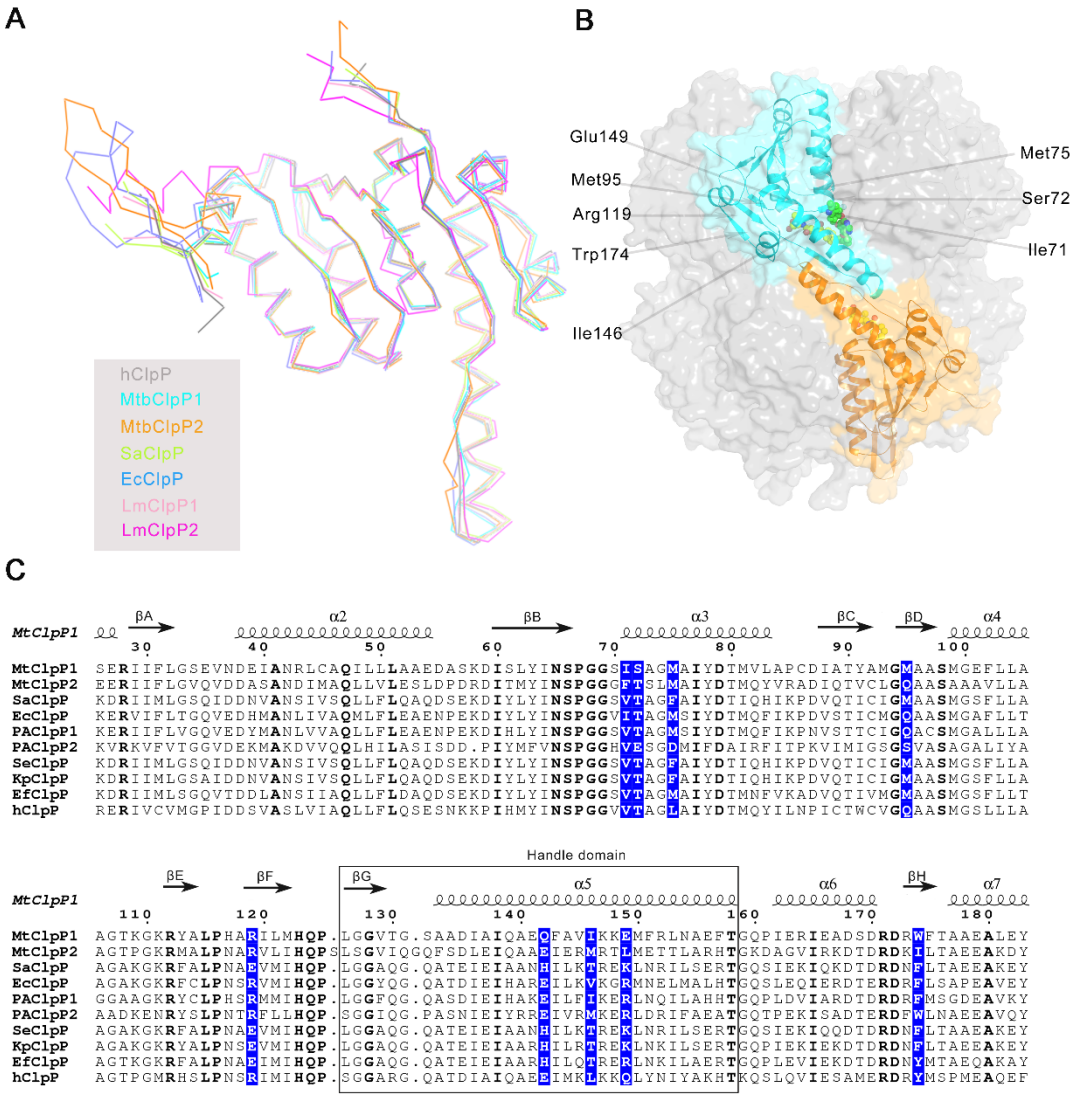

Figure 4

646 **S1 Table. Plasmids used in this study.**

Plasmid	Feature	Reference
pRSF-duet-1-*Mtb*ClpP1	For expressing *Mtb*ClpP1 protein	This study
pRSF-duet-1-*Mtb*ClpP2	For expressing *Mtb*ClpP2 protein	This study
pRSF-duet-1-*Ec*ClpP	For expressing *Ec*ClpP protein	This study
pRSF-duet-1-*Pa*ClpP1	For expressing *Pa*ClpP1 protein	This study
pRSF-duet-1-*Sa*ClpP	For expressing *Sa*ClpP protein	This study
pRSF-duet-1- *h*ClpP	For expressing *h*ClpP(ΔC) protein	This study

647

648

649 **S2 Table. Primers used in this study.**

Gene	Primers
*Mtb*ClpP1-Forword	CAGATTGGTGGATCCATGCGTTCGAACTCGC AG
*Mtb*ClpP1-Reverse	TTTACCAGACTCGAGTCACTGTGCTTCTCCA TTGAC
*Mtb*ClpP2-Forword	CAGATTGGTGGATCCCGCTACATCCTGCCGT CGTTC
*Mtb*ClpP2-Reverse	TTTACCAGACTCGAGTCAGGCGGTTTGCGCG GAGAG
RSF-duet-1-Forword	CTCGAGTCTGGTAAAGAAACCG
RSF-duet-1- Reverse	GGATCCACCAATCTGTTCTCTG
*h*ClpP- Forword	GAGAACAGATTGGTGGATCCCCGCTCATTCC CATCGTG
*h*ClpP- Reverse	GTTTCTTTACCAGACTCGAGGGTGCTAGCTG GGACAGGTTC
*Ec*ClpP- Forword	GAGAACAGATTGGTGGATCCATGTCATACA GCGGCGAAC
*Ec*ClpP- Reverse	GTTTCTTTACCAGACTCGAGTCAATTACGAT GGGTCAGAATC
*Pa*ClpP1- Forword	GAGAACAGATTGGTGGATCCATGTCTCGCA ACTCTTTTAT TC
*Pa*ClpP1- Reverse	GTTTCTTTACCAGACTCGAGTTAGACGGCCA G GTCGCGCTG
I71V- Forword	GTC AGCGCCGGCATGGCGATC
I71V- Reverse	CGATCCACCCGGCGAATTGAT
M75L- Forword	CTT GCGATCTACGACACCATG
M75L- Reverse	GCCGGCGCTGATCGATCCAC

M75D- Forword	GAC GCGATCTACGACACCATG
M75D- Reverse	GCCGGCGCTGATCGATCCAC
M95L- Forword	C TT GCCGC CTCGATGGGC GAG
M95L/W/S- Reverse	GCCCATCGCG TAGGTGGC
M95W- Forword	T GG GCCGC CTCGATGGGC GAG
M95S- Forword	TCG GCCGC CTCGATGGGC GAG
R119E- Forword-1	GAAATCCTGATGCACCAGCCG
R119E/Q/S-Reverse-1	AGCATGCGGCAGCGCGTAG
R119Q-Forword-1	CAG ATCCTGATGCACCAGCCG
R119S- Forword-1	TCG ATCCTGATGCACCAGCCG
R119E-Forword-2	GCTACGCGCTGCCGCATGCTGAAATCCTGAT GCACC AGCCGTTG
R119Q-Forword-1	GCTACGCGCTGCCGCATGCTCAGATCCTGAT GCACCAGCCGTTG
R119S- Forword-1	GCTACGCGCTGCCGCATGCTTCGATCCTGAT GCACC AGCCGTTG
R119E/Q/S-Reverse-2	AGCATGCGGCAGCGCGTAG
E142H- Forword	CACTTCGCCGTGATCAAGAAAG
E142H- Reverse	CTCGGCCTGGATGGCGATATC
E142R- Forword	CGC TTCGCCGTGATCAAGAAAG
E142R- Reverse	CTCGGCCTGGATGGCGATATC
I146V- Forword	GTCAAGAAAGAAATGTTCCGGC
I146V/L/T- Reverse	CACGGCGAACTGCTCGGC
I146L- Forword	C TT AAGAAAGAAATGTTCCGGC
I146T- Forword	ACT AAGAAAGAAATGTTCCGGC
E149L- Forword	CTTATGTTCCGGCTCAACGCCG
E149L/R/K/Q/T- Reverse	TTTCTTGATCACGGCGAACTG
E149R- Forword	CGC ATGTTCCGGCTCAACGCCG
E149K- Forword	AA G ATGTTCCGGCTCAACGCCG

E149Q- Forword	CAG ATGTTCCGGCTCAACGCCG
E149 T- Forword	ACT ATGTTCCGGCTCAACGCCG

650

651 **S3 Table. Strains used in this study.**

Strains	Feature	Source
E. coli strains DH5α	For amplification of plasmid	TransGen Biotech
E. coli strains BL21(DE3)	For expressing protein	TransGen Biotech
Staphylococcus aureus	MIC	ATCC33591 ATCC25923
Staphylococcus epidermidis	MIC	B27 ATCC12228
Enterococcus faecalis	MIC	ATCC33186
Enterococcus faecium	MIC	ATCC35667
Pseudomonas aeruginosa	MIC	ATCC27853 C58
Klebsiella pneumoniae	MIC	ATCC4352 ATCC700603
Escherichia coli	MIC	ATCC25922 ATCC35218
Mycobacterium smegmatis MC^{2}155	MIC	ATCC 700084
Mycobacterium tuberculosis H37Rv	MIC	ATCC 27294

652

653

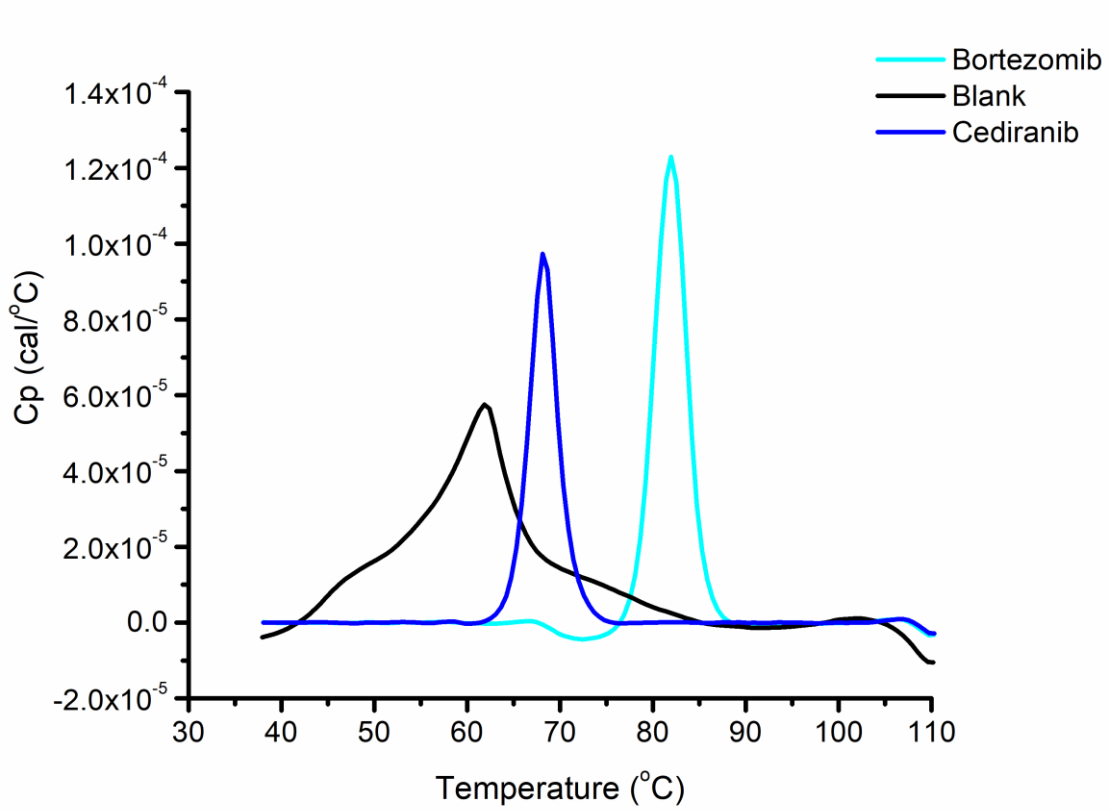

S1 Fig

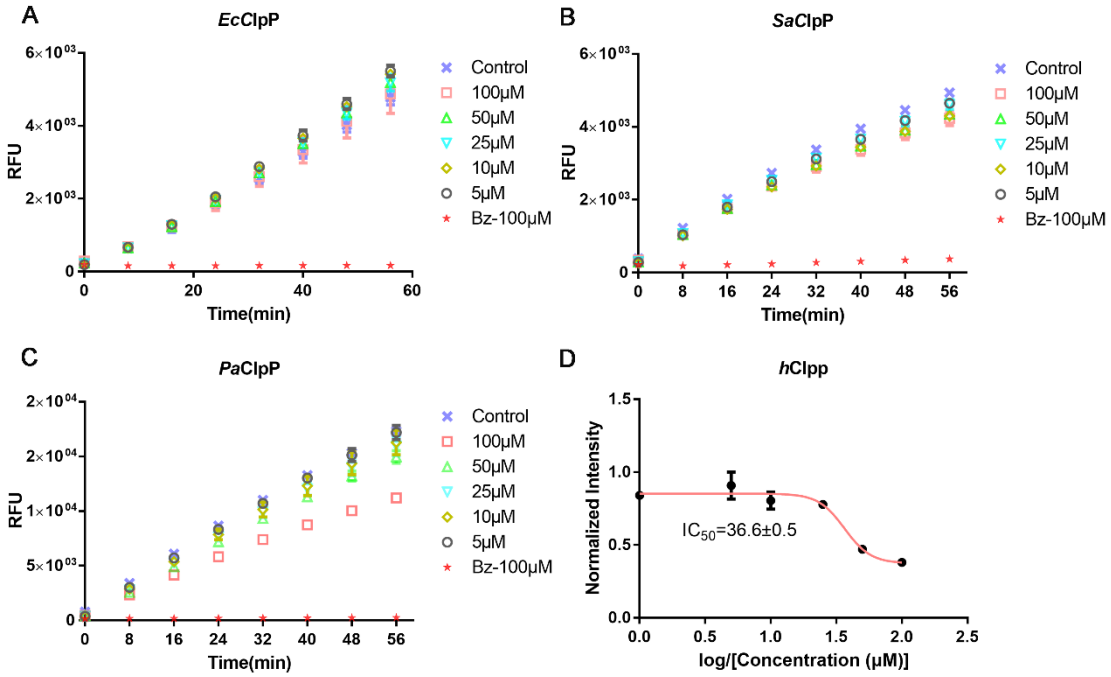

657

658 **S2 Fig**

659

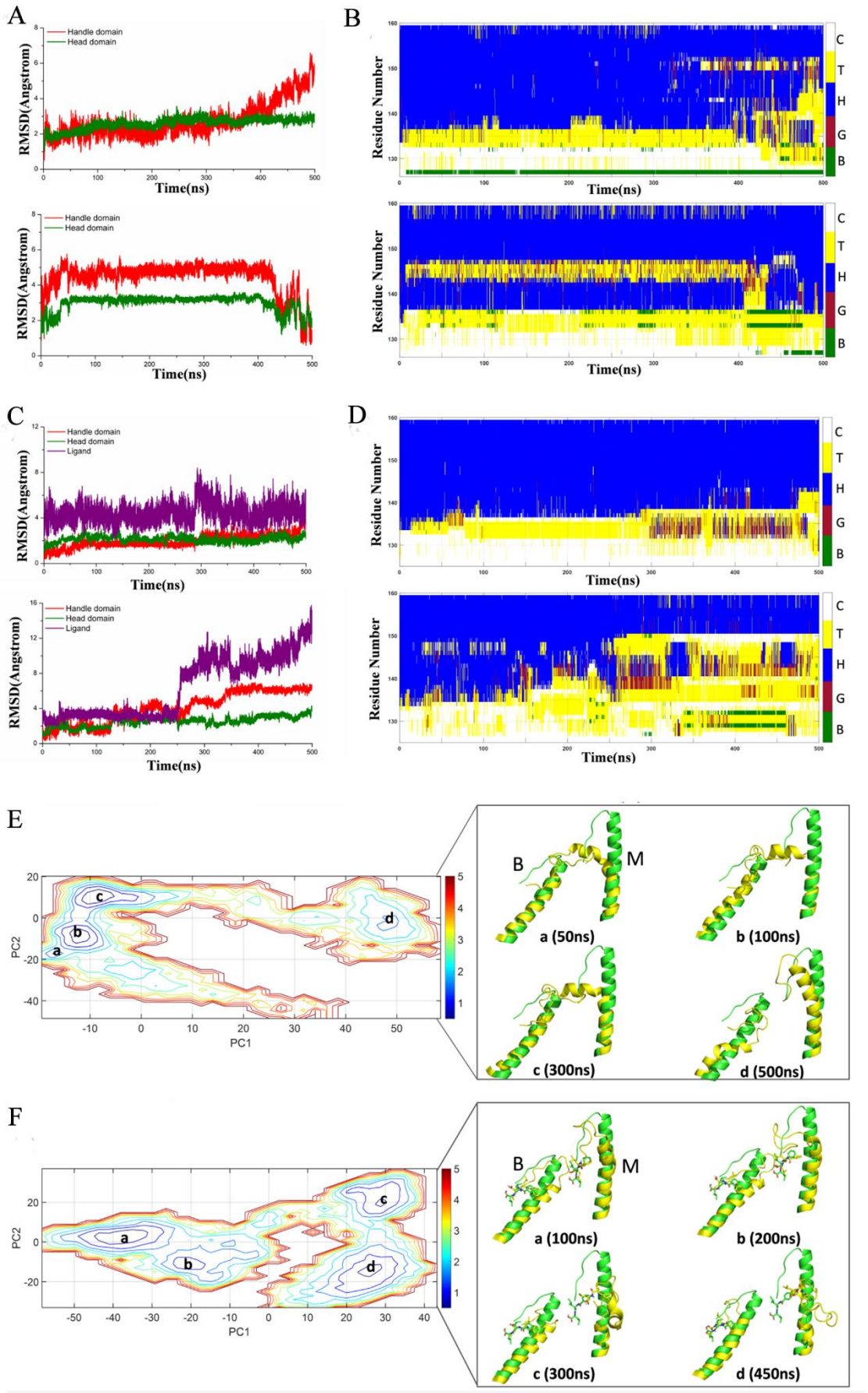

S3 Fig